symmetry

IMPACT FACTOR 2.2

CITESCORE 5.4

Review

Probing the Equation of State of Dense Nuclear Matter by Heavy Ion Collision Experiments

Peter Senger

Special Issue

Symmetry Energy in Nuclear Physics and Astrophysics

Edited by

Prof. Dr. Aziz Rabhi, Prof. Dr. Sidney Avancini and Prof. Dr. Mª Ángeles Pérez García

MDPI

https://doi.org/10.3390/sym16091162

symmetry

MDPI

Review

Probing the Equation of State of Dense Nuclear Matter by Heavy Ion Collision Experiments

Peter Senger

Facility for Antiproton and Ion Research GmbH, 64291 Darmstadt, Germany; p.senger@gsi.de

Abstract: The investigation of the nuclear matter equation of state (EOS) beyond saturation density has been a fundamental goal of heavy ion collision experiments for more than 40 years. First constraints on the EOS of symmetric nuclear matter at high densities were extracted from heavy ion data measured at AGS and GSI. At GSI, symmetry energy has also been investigated in nuclear collisions. These results of laboratory measurements are complemented by the analysis of recent astrophysical observations regarding the mass and radius of neutron stars and gravitational waves from neutron star merger events. The research programs of upcoming laboratory experiments include the study of the EOS at neutron star core densities and will also shed light on the elementary degrees of freedom of dense QCD matter. The status of the CBM experiment at FAIR and the perspective regarding the studies of the EOS of symmetric and asymmetric dense nuclear matter will be presented.

Keywords: heavy ion collision experiments; nuclear matter equation of state; QCD phase diagram

PACS: 29.40.Gx; 29.90 + r; 24.85 + p

Citation: Senger, P. Probing the Equation of State of Dense Nuclear Matter by Heavy Ion Collision Experiments. *Symmetry* **2024**, *16*, 1162. https://doi.org/10.3390/sym16091162

Academic Editors: Aziz Rabhi, Sidney Avancini and Mª Ángeles Pérez García

Received: 24 June 2024
Revised: 29 July 2024
Accepted: 1 August 2024
Published: 5 September 2024

1. Introduction

The fundamental physics goal of the pioneering experiments with high-energetic heavy ions was to explore the nuclear matter equation of state (EOS) at high densities. This motivation was triggered by the expectation that, in heavy ion collisions at beam energies up to 1 A GeV, the nucleons in the reaction volume will pile up to two to three times the saturation density ρ_0. In the early 1980s, the first beams of heavy nuclei were delivered by the Bevalac at LBL in Berkeley. The Plastic Ball collaboration discovered the collective flow of protons with respect to the reaction plane, which indicates stopping and pile-up of the nucleons, followed by an expansion of the compressed matter in the reaction volume [1]. The Streamer Chamber collaboration at LBL measured the excitation function of pion production and extracted the fireball temperature from the pion multiplicity. The interpretation of the experimental data by a thermal model allowed to separate the thermal energy from the compressional energy of the fireball. The result of this comparison was interpreted as an indication of a hard nuclear matter equation of state (EOS) [2]. On the other hand, according to a relativistic mean field model, the pion yield is more sensitive to in-medium effects than to the EOS [3].

Since the 1990s, the SIS18 synchrotron at GSI also provided Au beams up to kinetic energies of 1.5 A GeV. The FOPI collaboration explored the collective flow of protons and light fragments in heavy ion collisions. The collective flow of both protons and neutrons was measured in Au + Au collisions at 400 A MeV using a combination of the Four Pi (FOPI) detector and the Large Neutron Detector (LAND) [4]. This experiment provided the first information on the symmetry energy of nuclear matter beyond saturation density. In experiments with the Kaon Spectrometer (KaoS), the production of strange particles was observed for the first time in Au + Au collisions [5,6]. It turned out that kaon production at subthreshold beam energies is sensitive to the EOS up to about three times the saturation density [7]. At the same time, experiments at AGS measured the excitation function

of the collective proton flow up to 10 A GeV [8]. These data were used to extract the EOS for symmetric matter up to five times the saturation densities, though with a large uncertainty [9]. In 2016, the collective flow of protons and light fragments measured at GSI in Au + Au collisions at beam energies from 0.4 to 1.5 A GeV by the FOPI collaboration has been published and compared to results of IQMD transport model calculations [10]. In the same year, new experimental data on the elliptic flow of neutrons and charged particles measured simultaneously in Au + Au collisions at 0.4 A GeV have been published by the ASY-EOS collaboration. By comparing the data to the results of UrQMD calculations, the symmetry energy above the saturation density could be further constrained [11].

New information on the properties of dense nuclear matter was provided by the analysis and interpretation of recent astronomical observations. The discovery of neutron stars with masses of about two solar masses and beyond [12,13], the first measurements of neutron star radii together with their masses [14], and the detection of gravitational waves emitted from colliding and merging neutron stars [15] substantially improved the constraints on the high-density EOS.

In this paper, the status of laboratory experiments on the EOS for symmetric matter and the symmetry energy at densities beyond the saturation density will be briefly reviewed. Moreover, future experiments will be discussed, which will investigate new observables sensitive to the EOS for both symmetric and asymmetric nucleonic matter up to neutron star core densities. Under these conditions, however, even the nucleons are expected to overlap and melt into elementary degrees of freedom. The possible experimental signatures for a phase transition from hadronic matter to quark–gluon matter will not be discussed in this article.

2. The Nuclear Matter Equation of State

The nuclear matter equation of state is described by the pressure as a function of density ρ and the derivative of the binding energy per nucleon E/A with respect to the density at a constant temperature T:

$$P = \rho^2 \, \partial(E/A)/\partial\rho \,|_{T = const}$$

The binding energy per nucleon at zero temperature (T = 0) can be expressed as a function of the density and isospin asymmetry parameter δ by

$$E/A(\rho,\delta) = E/A(\rho,0) + E_{sym}(\rho)\cdot\delta^2 + O(\delta^4)$$

where the first term represents the EOS for symmetric matter and the second term the symmetry energy E_{sym} with the isospin asymmetry parameter $\delta = (\rho_n - \rho_p)/\rho$. For symmetric matter, the binding energy has a minimum value of $E/A(\rho_0,0) = -16$ MeV at the saturation density ρ_0 and a curvature at ρ_0 denoted as nuclear matter incompressibility:

$$K_{nm} = 9\rho^2 \cdot \partial^2(E/A)/\partial\rho^2$$

The symmetry energy can be parameterized as

$$E_{sym}(\rho) = E_{sym}(\rho_0) + L(\rho_0)/3((\rho - \rho_0)/\rho_0)$$

with $L(\rho_0) = 3\rho \, \partial E_{sym}/\partial\rho$ at $\rho = \rho_0$ describing the slope of the symmetry energy at the saturation density.

The left panel in Figure 1 depicts various calculations of the binding energy per nucleon for symmetric and antisymmetric nuclear matter as a function of density, whereas, in the right panel of Figure 1, the symmetry energy, i.e., the difference of the respective curves shown in the left panel, is plotted [16].

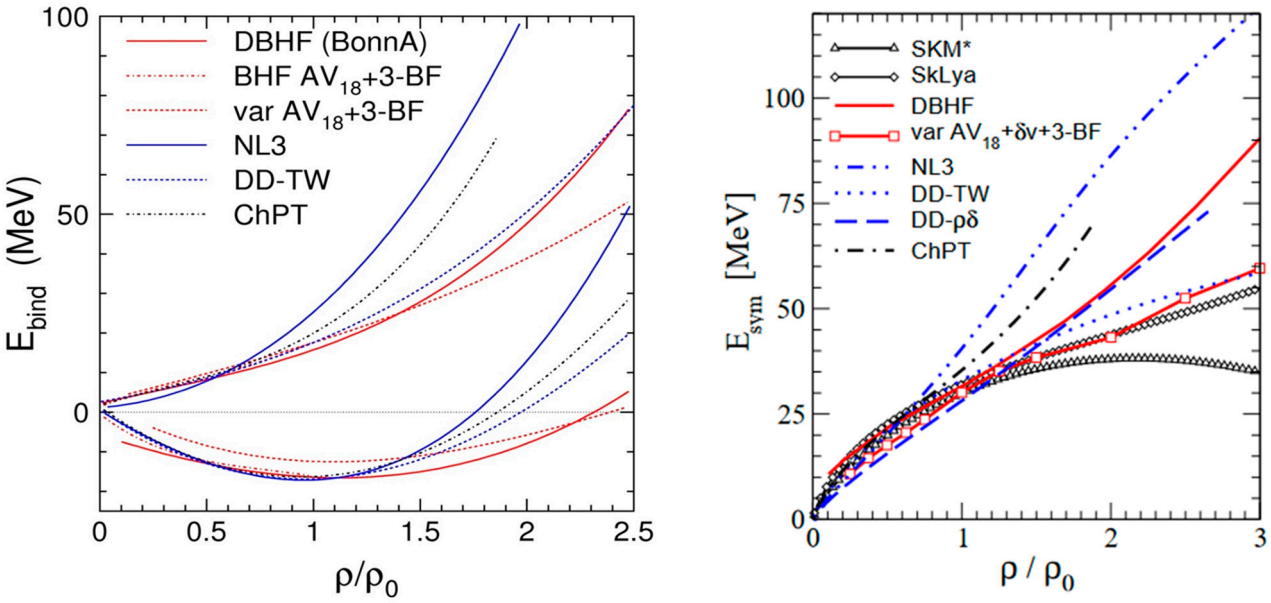

Figure 1. Left panel: EOS of isospin-symmetric nuclear matter (lower curves) and neutron matter (upper curves). E_{bind} corresponds to E/A in the text. **Right** panel: symmetry energy as a function of density. BHF/DBHF and variational calculations are compared to phenomenological density functionals NL3 and DD-TW and ChPT [16].

Many laboratory experiments have been performed to investigate the EOS below or close to the saturation density. For example, theoretical calculations reproducing experimental results on the Giant Monopole Resonance in ^{208}Pb extracted values of $194 < K_{nm} < 240$ MeV for the nuclear incompressibility of symmetric nuclear matter around the saturation density [17]. Also, the symmetry energy was investigated in various experiments, from which averaged values for $E_{sym}(\rho_0) = 31.6$ MeV and $L(\rho_0) = 58.9$ MeV for the slope parameter were extracted [18]. Recently, the neutron skin thickness of ^{208}Pb and ^{48}Ca has been measured by PREX and CREX experiments, respectively. A combined Bayesian analysis of these results found values of $E_{sym}(\rho_0) = 30.2 + 4.1 - 3.0$ MeV and $L(\rho_0) = 15.3 + 46.8 - 41.5$ MeV at the 90% confidence level [19].

3. Experiments on the EOS of Symmetric Nuclear Matter at High Density

The first robust extraction of the compressibility modulus K of nuclear matter has been made possible by studying the multiplicity ratio of K^+ production in heavy (Au + Au) over light (C + C) nuclei at incident energies from 0.6 to 1.5 A GeV by the KaoS Collaboration [20–22]. At these energies, K^+ mesons cannot be produced in direct nucleon–nucleon collisions like $NN \rightarrow N\Lambda K^+$, because, in this case, the threshold beam energy is $E_{lab} = 1.58$ GeV. According to transport models, the kaons are created via subsequent collisions of protons, neutrons, and pions, and the probability of those multiple collisions increases with the increasing density of the reaction volume. Therefore, "subthreshold" K^+ production is sensitive to the compressibility of nuclear matter. Moreover, K^+ mesons, which consist of an anti-s and an up-quark, cannot be absorbed by the surrounding nucleons due to strangeness conservation. Hence, K^+ mesons can be regarded as "penetrating" probes of the dense fireball created in heavy ion collisions, as their mean free path in nuclear matter is rather long, about 7 fm. Final state interactions such as elastic K^+N scattering do not change the K^+ multiplicity.

The data could be reproduced by microscopic Relativistic Quantum Molecular Dynamics (RQMD) calculations, taking into account in-medium kaon potentials calculated by the Chiral Perturbation Theory and assuming a nuclear incompressibility of $K_{nm} = 200$ MeV [23]. The investigation of an excitation function allows to probe different densities. Moreover, the comparison to a light reference system partially cancels systematic background contribu-

tions to subthreshold kaon production from Fermi momenta and short-range correlations and reduces the effects of theoretical uncertainties concerning in-medium cross-sections and momentum-dependent interactions. Figure 2 depicts the experimental data together with the results of three different transport models assuming a "soft" EOS with a nuclear incompressibility of K_{nm} = 200 MeV (red symbols) and a "hard" EOS with K_{nm} = 380 MeV (blue symbols). The figure illustrates that the sensitivity of subthreshold particle production to the EOS increases with the decreasing beam energy, i.e., if subsequent particle interactions are required to accumulate the energy needed for the production of a kaon.

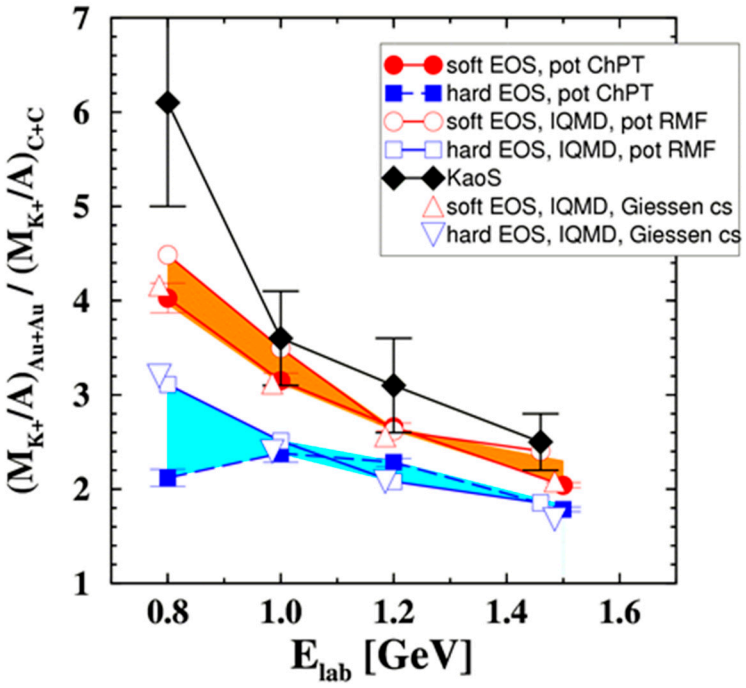

Figure 2. Ratio of the K^+ multiplicity per mass number of the colliding nuclei (Au = 197, C = 12) in Au + Au normalized to C + C collisions as a function of the beam energy (black symbols). The data are compared to different QMD calculations assuming a soft EOS (K_{nm} = 200 MeV, red symbols) or a hard EOS (K_{nm} = 380 MeV, blue symbols). Taken from [23].

A more direct observable sensitive to the nuclear matter EOS beyond the saturation density is the collective flow of particles driven by the pressure gradient in the reaction volume of a heavy ion collision. Pioneering experiments have been performed at the Alternating Gradient Synchrotron (AGS) at Brookhaven National Laboratory (BNL), where both the transverse and the elliptic proton flow has been measured by various experiments in Au + Au collisions at beam kinetic energies from 2 to 11 A GeV [8]. The experimental data have been compared to relativistic transport model calculations, which take into account in-medium cross-sections and a momentum-dependent mean field [9]. It turns out that the transverse flow data can be reproduced with the assumption of a soft EOS with an incompressibility of $K_{nm} \approx 210$ MeV, while the elliptic flow data agree better in simulations with a hard EOS ($K_{nm} \approx 300$ MeV). Figure 3 depicts the results of the calculations of the elliptic flow for different incompressibility values together with the AGS data shown by the black symbols. According to these calculations, the fireball produced at the highest beam energies will be compressed to net-baryon densities of 6–7 ρ_0 and thus reach densities similar to those in the core of neutron stars. These microscopic transport codes assume that there is no significant explicite temperature dependence of the interactions, except for the thermal particle momenta, which are taken into account by the scattering of the particles.

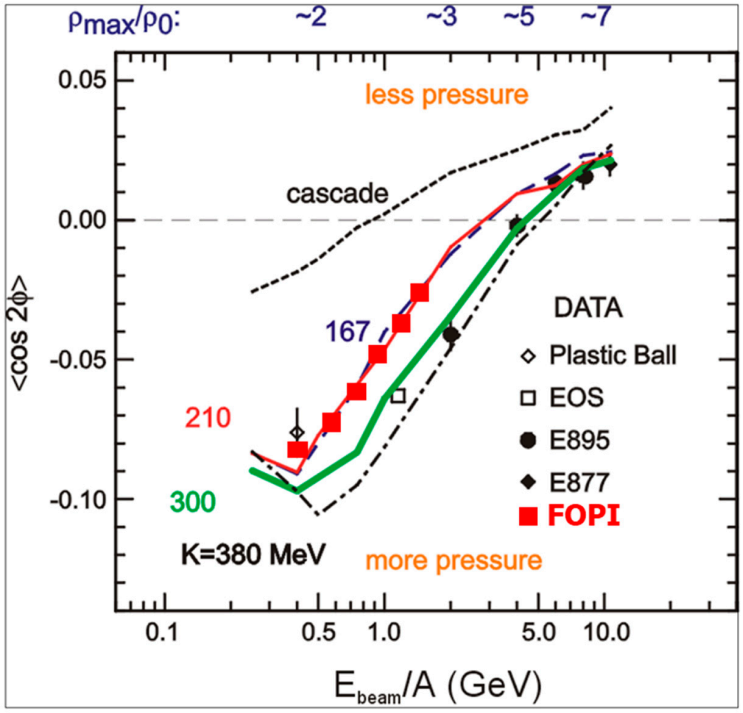

Figure 3. Elliptic flow as a function of the beam energy measured in heavy ion collisions (symbols) compared to the results of the relativistic transport model calculations for different values of the nuclear incompressibility [9]. The black symbols represent the results of the experiments at AGS (for details, see [9]). The FOPI/GSI results represented by red symbols [10] were included in the figure taken from [9]. The short-dashed black line ("cascade") corresponds to calculations without EOS, and the long-dashed black line, the red line, the green line, and the dashed dotted line represent the results of calculations assuming nuclear incompressibilities of K_{nm} = 167, 210, 300, and 380 MeV, respectively.

More than a decade later, the FOPI collaboration at GSI has performed systematic measurements of the elliptic flow of protons, deuterons, tritons, and ^{3}He-nuclei in Au + Au collisions at energies from 0.4 to 1.5 A GeV [10]. In those collisions, the reaction volume is compressed to about twice the saturation density. The experimental elliptic flow values have been reproduced by IQMD transport model calculations, assuming a nuclear incompressibility of K_{nm} = 190 ± 30 MeV, in agreement with the KaoS result ($K_{nm} \approx$ 200 MeV; see Figure 2). The IQMD model also takes into account momentum-dependent interactions and in-medium cross-sections. As illustrated in Figure 3, the FOPI data improve the data situation and indicate that the new elliptic flow data up to densities of about 2 ρ_0 also point towards a soft EOS, like the experimental data on the transverse flow.

4. Symmetry Energy above the Saturation Density

Using an improved experimental setup, the ASY-EOS collaboration at GSI measured the elliptic flow of neutrons and charged particles in Au + Au collisions at 400 MeV/nucleon [24]. At these beam energies, nuclear densities between $0.8 < \rho/\rho_0 < 1.6$ are reached. The experimental data have been compared to simulations using the UrQMD transport code, which includes momentum-dependent interactions. The measured ratio of the elliptic flow of neutrons over the elliptic flow of charged particles v_2^n/v_2^{ch} could be reproduced by assuming a soft EOS, a value for the symmetry energy at a saturation energy of $E_{sym}(\rho_0)$ = 31 MeV, and a slope parameter of $L(\rho_0)$ = 72 ± 13 MeV [11]. The resulting extrapolation of the symmetry energy towards higher densities is illustrated in Figure 4 (red band), together with the FOPI-LAND result $L(\rho_0)$ = 83 ± 26 [4,24] (yellow band). Moreover, the figure includes the results of the analysis of neutron skins in ^{208}Pb [25], isospin diffusion

data and neutron/proton double ratios measured in Sn + Sn collisions at 50 A MeV [26], and isobar analog states. For a review, see [27].

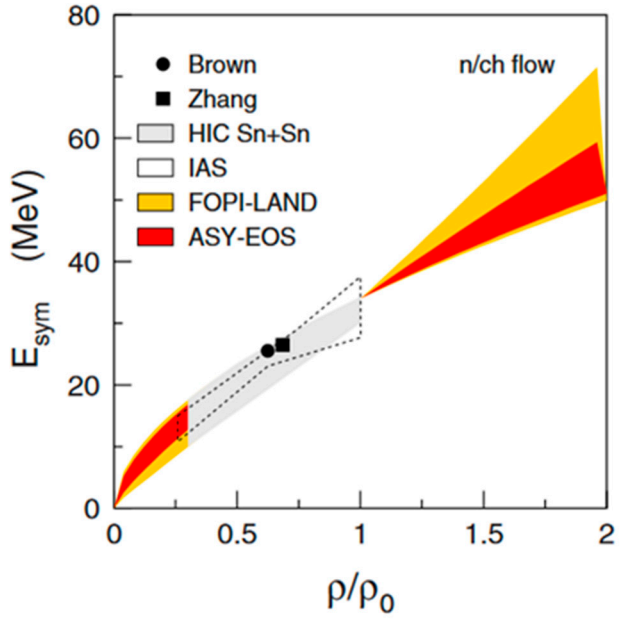

Figure 4. Constraints for the symmetry energy as a function of normalized nuclear density ρ/ρ_0 [23–27]. The FOPI-LAND [4,24] and the ASY-EOS [11] results are not shown in the range $0.3 < \rho/\rho_0 < 1.0$.

Recently, symmetry energy has been studied by measuring the π^-/π^+ spectral ratio in isospin asymmetric ^{132}Sn + ^{124}Sn and ^{108}Sn + ^{112}Sn collisions, both at a beam kinetic energy of 270 A MeV. At these energies, the pions are partly produced above the saturation density. The comparison of the data to the results of the dcQMD transport model calculations allowed to constrain the symmetry energy at the saturation density to values of $32.5 < E_{sym}(\rho_0) < 38.1$ MeV and the slope parameter at the saturation density to values of $42 < L(\rho_0) < 117$ MeV [28]. In order to improve the reliability of the various transport models, the groups working on these models have founded the Transport Model Evaluation Project (TMEP), with the aim to test the robustness and consistency of the model predictions [29].

The existing information on the EOS for symmetric and neutron matter extracted from heavy ion collision experiments for nuclear densities up to about 2 ρ_0 is presented as green areas in Figure 5, which also contains results of ab initio calculations for the EOS of symmetric matter (lower set of curves) and for neutron matter (upper set of curves) [7]. The figure depicts the binding energy per nucleon as a function of the baryonic density. The lower green band illustrates the EOS for symmetric matter based on the analysis of the experimental results from KaoS [20–22] and FOPI [10]. The upper green band illustrates the EOS for neutron matter, which is obtained by the sum of the binding energy in symmetric matter (results from KaoS and FOPI) and the symmetry energy (result from ASY-EOS [11]). In conclusion, the upper green band in Figure 5 represents the up-to-date experimental constraint for the EOS for neutron matter up to twice the saturation density.

Finally, the results from the laboratory experiments are plotted together with the data from the astrophysical observations in Figure 6, which depicts the pressure as a function of the density for neutron matter. As mentioned in the Introduction, constraints on the high-density equation of state (EOS) have been obtained from the measurement of the masses of massive neutron stars [12,13], from simultaneous measurements of the radii and masses of neutron stars [14], and from the detection of gravitational waves emitted from neutron star mergers [15]. The result of a combined analysis of these astronomical data is presented in Figure 6, together with the combined results of the GSI experiments FOPI, KaoS, and ASY-EOS and the analysis of the AGS flow data after adding the symmetry energy with

a strong and a weak density dependence, respectively [9]. Figure 6 illustrates that, up to densities of about 2 ρ_0, the EOS is constrained by heavy ion collision results, while, at higher densities, new heavy ion measurements are required to improve the data situation.

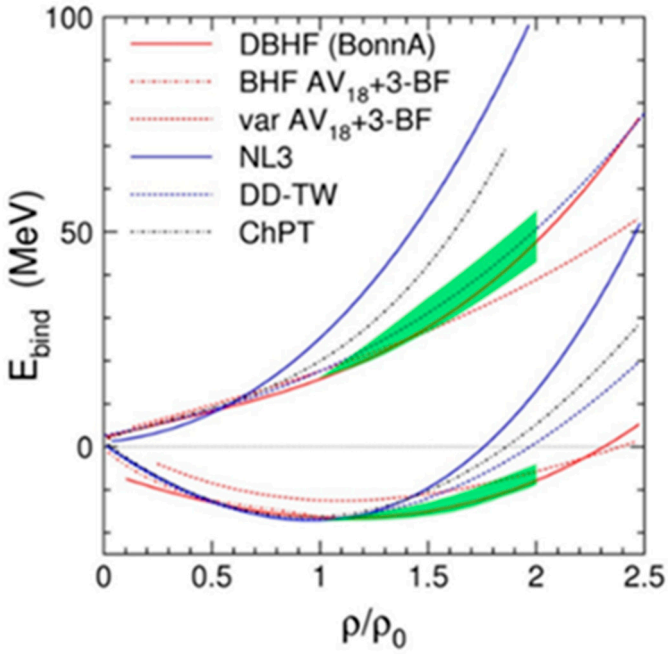

Figure 5. Binding energy versus normalized baryon density calculated by microscopic ab initio calculations [7]. Lower set of curves: EOS of isospin-symmetric nuclear matter. Upper set of curves: EOS of pure neutron matter. Lower green area: EOS extracted by UrQMD and RQMD calculations from experimental data taken at GSI by FOPI [10] and KaoS [20–22]. Upper green area: Sum of the EOS for symmetric matter and the symmetry energy extracted by UrQMD calculations from n/p flow data measured by the ASY-EOS experiment [11]. Adapted from [7].

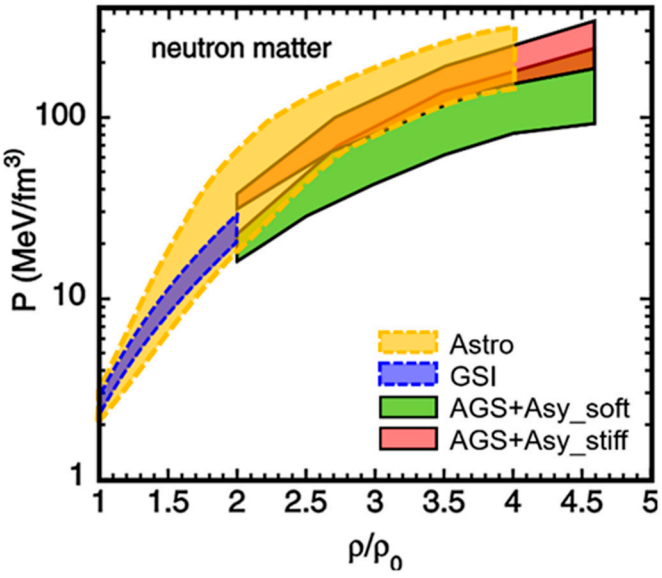

Figure 6. EOS for cold neutron matter plotted as pressure versus density. Orange area: Analysis of the masses and radii of neutron stars measured by NICER, including mass measurements of the most massive neutron stars, and the tidal deformability estimate from the GW170817 [4]. Blue area: Analysis of the GSI flow and kaon data [8–10,15]. Pink and green area: Analysis of AGS flow data [11–13] after adding the pressure from asymmetry terms with strong and weak density dependences, respectively.

5. Constraining the EOS at Neutron Star Core Densities

The large uncertainty of the pressure extracted from heavy ion data above about twice the saturation density, as illustrated in Figure 6, requires further precise measurements of the excitation function of the collective flow of identified particles in heavy ion collisions at beam energies from 2 to 10 A GeV, where nuclear densities above 5 ρ_0 can be reached (see Figure 3). Moreover, the investigation of additional, flow-independent observables is highly desirable. Microscopic transport calculations have demonstrated, based on the data measured at GSI, that the subthreshold strangeness production of strange particles is a powerful tool to study the high-density EOS of symmetric matter. In order to expand this method to higher densities, both the beam energy and the particle production thresholds have to be increased. Obvious candidates for diagnostic probes at higher beam energies are multi-strange (anti-) hyperons, like $\Xi^{\pm}$ and $\Omega^{\pm}$ hyperons, which have production thresholds in proton–proton collisions ranging from 3.7 GeV (Ξ^-) to 12.7 GeV(Ω^+). Similar to K mesons at lower beam energies, these particles are also produced in sequential hadronic collisions and strangeness exchange reactions involving kaons, lambdas, and sigma-hyperons [30,31]. Therefore, the yields of multi-strange hyperons produced at subthreshold beam energies are enhanced at high densities, which opens up the possibility to study the EOS. The information on the EOS will be obtained by a comparison of the experimental data to the results of microscopic transport calculations, which should take into account momentum-dependent interactions and in-medium hyperon potentials. However, the importance of in-medium hyperon potentials decreases with the increasing density, as repulsive interactions become dominant. Moreover, by comparison to reference measurements, the influence of such effects on particle production can be additionally reduced, as discussed above for the case of K-mesons.

The sensitivity of subthreshold hyperon production on the EOS of isospin symmetric matter has been studied in simulations with the PHQMD transport code for central Au + Au collisions at a beam energy of 4 A GeV [32]. Figure 7 presents the result of this calculation as ratios of the yields of multi-strange (anti-) hyperons for a soft over a hard EOS, plotted against their production threshold energy in p + p collisions. As expected, the yield of the produced hyperons is higher for a soft EOS than for a hard EOS, because, in the case of a soft EOS, the fireball is compressed to higher densities, which enhances the number of sequential collisions producing hyperons. The yield ratio increases with the increasing production threshold of the hyperons, starting from Ξ^-(soft EOS)/Ξ^-(hard EOS) = 1.5 to Ω^+(soft EOS)/Ω^+ (hard EOS) = 2.5. As a reference, the yield of multi-strange hyperons was also calculated in C + C collisions, where the hyperon yields do not exhibit a dependence on the EOS. By measuring the yield ratios of hyperons in Au + Au over C + C collisions, not only the systematic uncertainties of both the measurement and the simulations are reduced but also the physical effects relevant for subthreshold particle production like the Fermi energy of the nucleons, in-medium modifications, and short-range correlations, largely cancel out in the ratio. The experimental challenge is to measure multi-strange (anti-)hyperons also in C + C collisions with very good statistics. Up to now, no systematic measurement of multi-strange hyperons has been performed in heavy ion collisions at beam energies that will be available at the future Facility for Antiproton and Ion Research (FAIR), i.e., between 2 and 11 A GeV.

In order to contribute to our understanding of neutron stars, the symmetry energy also has to be determined for nuclear matter at baryon densities of up to about 5 ρ_0. One possibility is to extend the simultaneous measurement of the elliptic flow of neutrons and protons to higher energies. Alternatively, information on the high-density E_{sym} can be extracted from the ratio of Σ^-(dds) over Σ^+(uus) hyperons [33]. These particles differ in the third component of the isospin $I_3 = \pm 1$ and reflect the density of neutrons (ddu) and protons (uud). However, the identification of $\Sigma^{\pm}$ hyperons is a challenging experimental task, because one of the decay products is a neutral particle. An experimental approach to identify $\Sigma^{\pm}$ hyperons is described in Section 6.

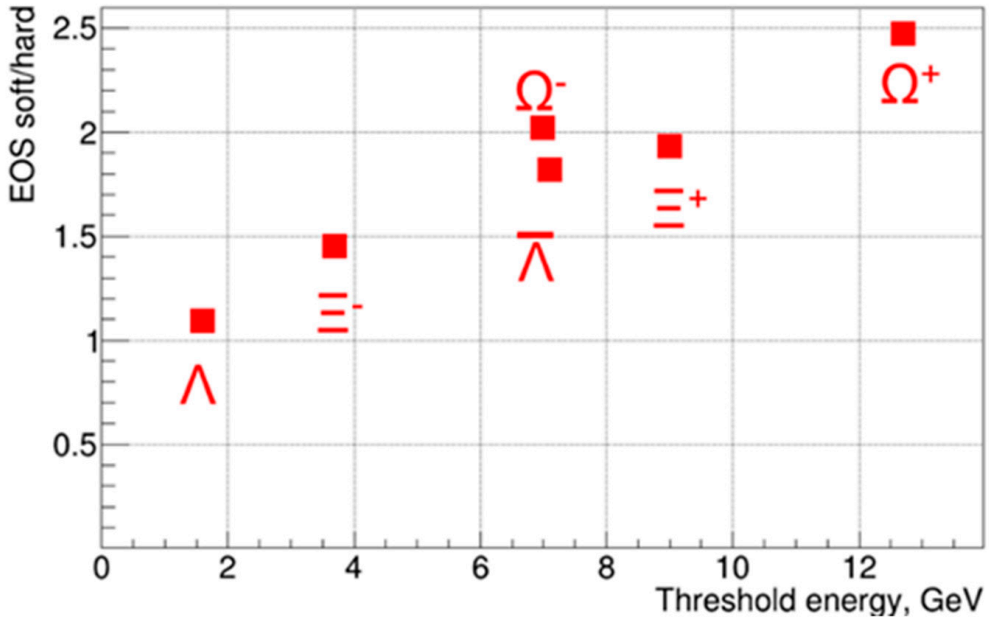

Figure 7. Ratios of (anti-)hyperon yields calculated with the PMQMD transport code for a soft over a hard EOS for central Au + Au collisions at a beam energy of 4 A GeV as a function of the production threshold in nucleon–nucleon collisions [32].

The experimental investigation of observables sensitive to the EOS for symmetric matter and to the symmetry energy at high baryon densities is an important part of the research program of the Compressed Baryonic Matter (CBM) experiment at FAIR in Darmstadt/Germany. These data will complement the results of future astronomical observations and help to further constrain the EOS of neutron stars. Another fundamental question is related to the microscopic structure of matter at neutron star core densities. Around densities of 5 ρ_0, the nucleons are expected to overlap, and model calculations predict a transition from nucleons to quarks and gluons. At which density such a transition occurs, and whether it is smooth and continuous or of the first order with a phase coexistence and critical endpoint, is one of the most interesting questions of dense matter physics, which can probably only be answered in heavy ion collision experiments. Lattice QCD (lQCD) calculations predict that the temperature of a critical endpoint of a first-order chiral phase transition has to be below $T_c = 132 + 3 - 6$ MeV [34], and more recent lQCD calculations find values for the critical temperature of $T_c \approx 100$ MeV at baryon chemical potentials of $\mu_{Bc} \approx 580$ MeV [35]. Calculations based on Dyson–Schwinger Equations and the Functional Renormalization Group (DSE-FRG) result in a critical endpoint temperature of $T_{cep} = 93$ MeV at a baryon chemical potential $\mu_{Bcep} = 672$ MeV [36]. These values are located in a region of the QCD phase diagram, which will be covered by FAIR energies and investigated by the CBM experiment.

6. The CBM Experiment at FAIR

The working horse of the future, "Facility for Antiproton and Ion Research" (FAIR), is a synchrotron with a magnetic rigidity of 100 Tm (SIS100), which delivers proton beams up to kinetic energies of 29 GeV with intensities up to 3×10^{13}/s, and heavy ion beams with kinetic energies from 2 A to 11 A GeV for Au or U nuclei with intensities up to 10^{10}/s. The beams can be delivered to a superconducting fragment separator (SFRS), where rare isotope beams will be produced and transported to high-energy beam (HEB) experiments, which study the properties of these isotopes in order to explore the origin of heavy elements. The SIS100 beams will also be delivered to the cave of the CBM experiment, where the properties of dense baryonic matter will be investigated. The SFRS and the CBM experiment will be realized in the first stage of the FAIR project, as illustrated by the green lines in Figure 8. As

the next step, as indicated by the blue lines in Figure 8, the experimental areas for the study of low-energy beams from the SFRS and the cave for the APPA (Atomic, Plasma Physics and Applications) experiments will be realized (applications include radiation biology and material science). FAIR will be completed by the construction of the collector ring (CR) and the high-energy storage ring (HESR), where hadron physics experiments will be performed with antiproton beams by the PANDA (AntiProton ANnihilation at DArmstadt) setup. The antiproton production target is located in a cave close to the APPA facility and will be bombarded by a high-intensity proton beam from a linear accelerator in front of the SIS18 synchrotron. These facilities are sketched by the brownish lines in Figure 8. The detailed FAIR research program was reviewed in [37].

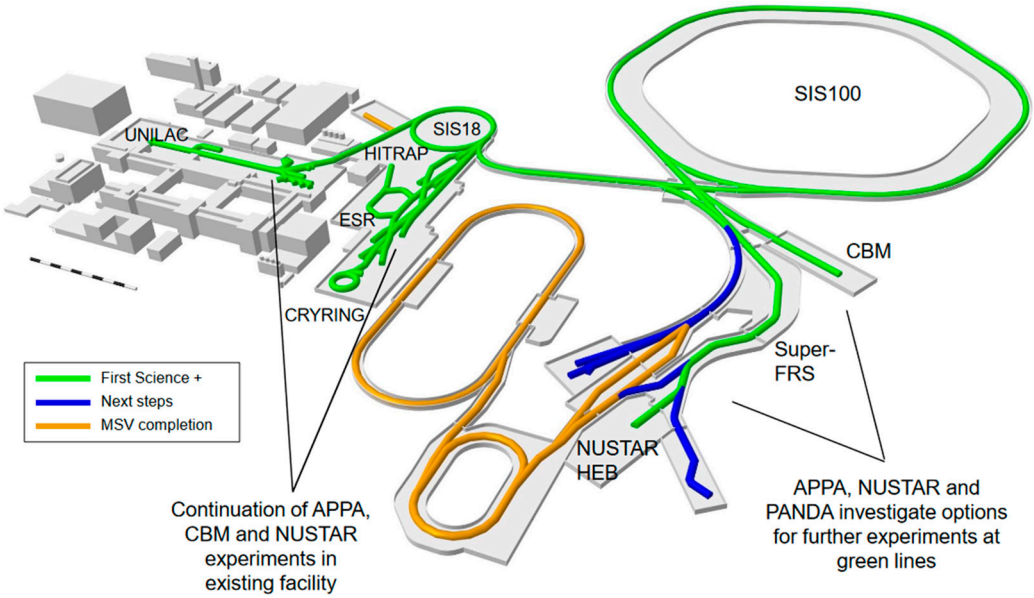

Figure 8. Sketch of the Facility for Antiproton and Ion Research indicating the different construction stages. Green lines: the existing GSI facilities together with the first FAIR stage, including the super fragment separator (SFRS) with its high-energy beam experimental (HEB) area and the CBM experiment. Blue Lines: The low-energy experiments downstream the SFRS and the APPA facilities. Brownish lines: The collector ring (CR), the high-energy storage ring (HESR) together with the PANDA experiment, and the proton accelerator in front of the SIS18 synchrotron of GSI [38].

The mission of the CBM experiment is the exploration of the fundamental properties dense baryonic matter, as it exists in the core of neutron stars and in the collision zone of neutron star mergers. In particular, the CBM physics program includes:

- The investigation of the nuclear matter equation of state at high baryon densities by measuring the excitation function of multi-strange hyperon production for different collision systems and the collective flow of particles.
- The search for a chiral crossover or a first-order phase transition, including its critical endpoint and the region of phase coexistence. Promising observables are event-by-event fluctuations of conserved quantities (baryons, strangeness, and charge) and the invariant mass spectra of dileptons, which allow to extract the fireball temperature and, hence, the caloric curve of strongly interacting matter when measuring an excitation function.
- Searching for signatures for chiral symmetry restoration, for example, the degeneration of chiral partners like the rho vector meson and the a1 axial vector meson, by measuring the dilepton invariant mass spectrum.
- Studying the production, the mass, and the collective flow of (double-) lambda hypernuclei in heavy ion collisions.

At FAIR beam energies, most of the diagnostic observables mentioned above are produced with very low cross-sections, and in order to measure these rare probes with high statistics and precision, the experiment has to run with unprecedented data rates of up to 10 MHz. This requires high-rate detectors with triggerless front-end electronics and free streaming data acquisition together with high-speed software algorithms running at the GSI Green-IT Cube and providing online track and event reconstruction and selection.

The CBM experimental setup is sketched in Figure 9. Charged hadrons will be identified by determination of their mass. This includes the measurement of the curvature of their tracks in a magnetic field, which provides the momentum, and the measurement of their time of flight, which provides the velocity. The tracks are measured by two silicon detector systems located in the large gap of a superconducting dipole magnet. The Micro-Vertex Detector (MVD) consists of four stations equipped with Monolithic Active Pixel Sensors (MAPSs), followed by the eight stations of the Silicon Tracking System (STS) comprising more than 900 double-sided microstrip sensors. The measured decay topology of short-lived particles such as hyperons allows to reconstruct the mass of the mother particle. The time of flight (TOF) wall consists of Multi-Gap Resistive Plate Chambers (MRPCs) covering an active area of 120 m^2 located about 8 m downstream the target. The identification of electrons is performed by a Ring Imaging Cherenkov (RICH) detector positioned downstream the magnet, together with a Transition Radiation Detector (TRD) downstream the RICH and in front of the TOF wall. In the case of muon measurements, the RICH will be replaced by a Muon Chamber (MuCh) system, consisting of up to five hadron absorbers with tracking chamber triplets in between two Gaseous Electron Multiplier (GEM) detector triplets and two Resistive Plate Chamber (RPC) triplets. The CBM detector systems cover polar emission angles from 3 to 25 degrees in order to cover the midrapidity at SIS100 beam energies. In order to determine the collision centrality and the orientation of the reaction plane, a Forward Spectator Detector (FSD) will measure the spectator fragments. It consists of plastic scintillator modules and is located about 10 m downstream the target. The status of the detector construction, the software development, and the results of the simulations are presented in the CBM Progress Report 2022 [39].

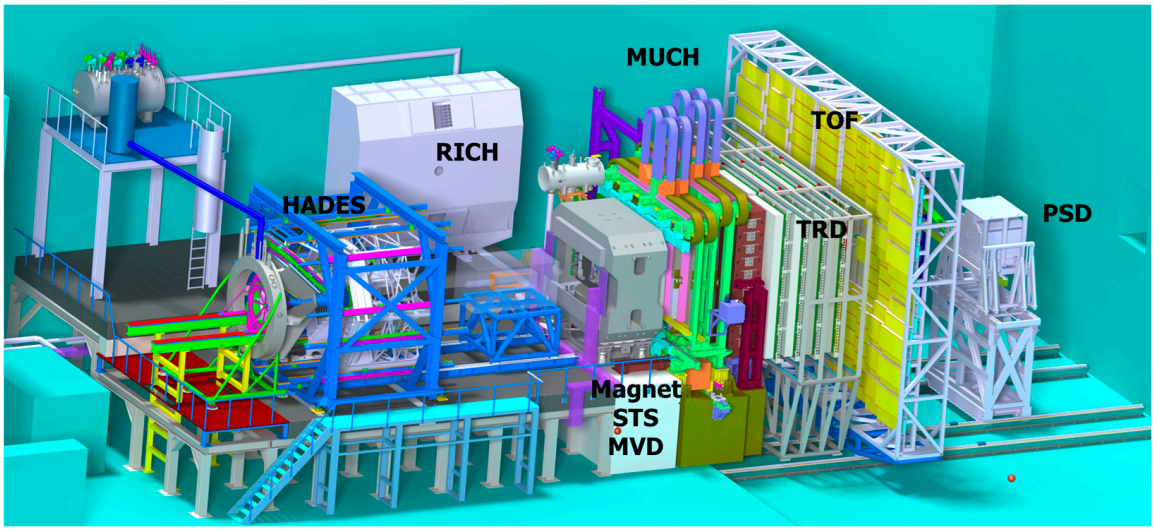

Figure 9. The detector setup for heavy ion collision experiments at FAIR; the beam enters from left side. Left: The HADES detector inside its blue support frame. Right: The CBM experiment consisting of the superconducting magnet hosting the Micro-Vertex Detector (MVD) and the Silicon Tracking System (STS). The Ring Imaging Cherenkov detector for electron identification is in the parking position, while the Muon Chambers (MUCHs) are in the measuring position, followed by the Transition Radiation Detector (TRD), the time of flight (TOF) wall, and the Projectile Spectator Detector (PSD).

In the following section, some results of the performance simulations concerning observables sensitive to the EOS will be presented. As discussed above, the yield of multi-strange hyperons produced at subthreshold beam energies is sensitive to the density of the reaction volume and, hence, to the EOS. Figure 10 depicts the invariant mass distributions of Lambda, anti-Lambda, anti-Xi, and Omega hyperons, reconstructed from their decay products, as simulated for central Au + Au collisions at a kinetic beam energy of 11 A GeV [40].

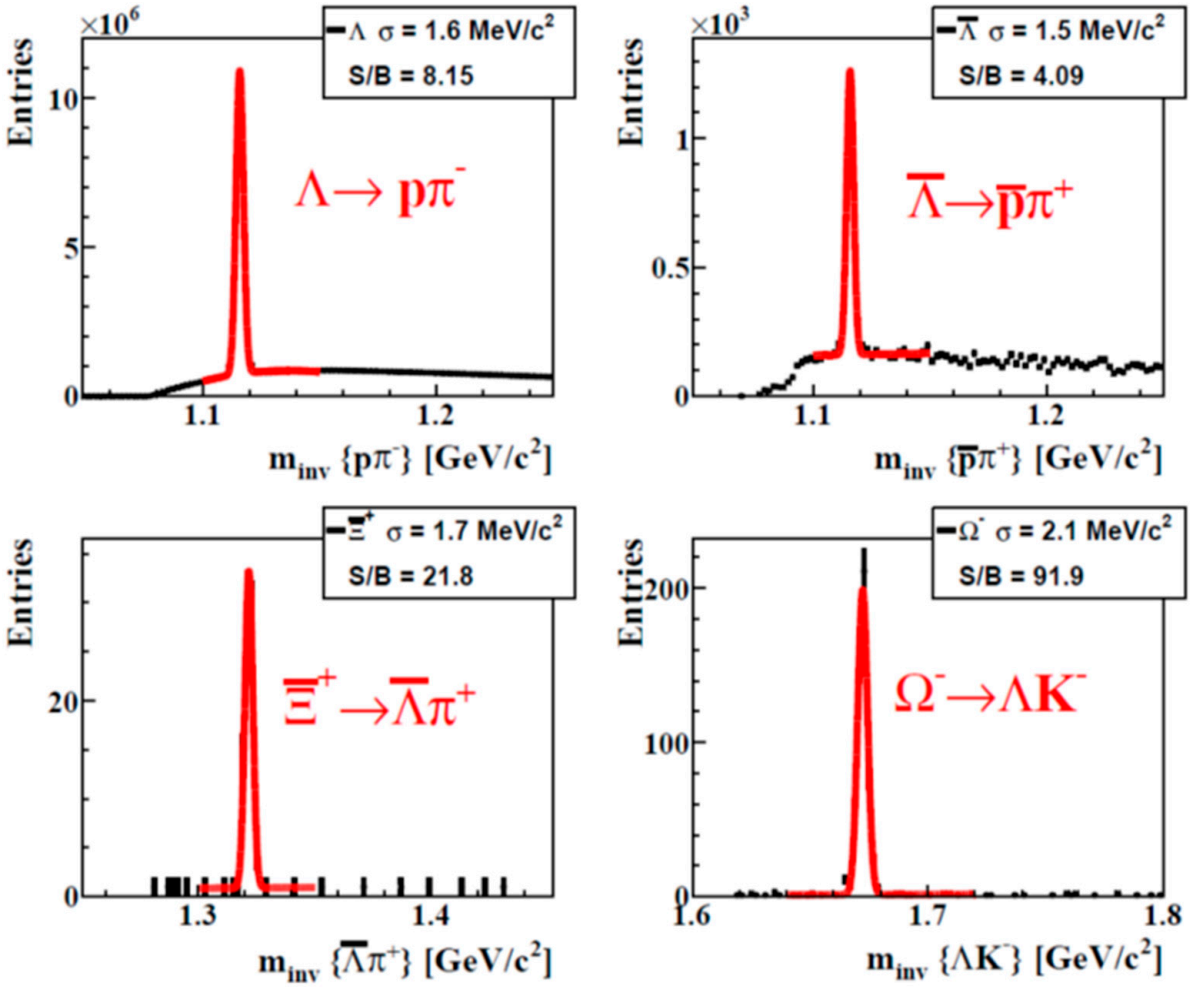

Figure 10. Invariant mass distribution of Λ, anti-Λ, Ξ^+, and Ω^- reconstructed from their daughter particles simulated for central Au + Au collisions at a beam energy of 11 A GeV [39].

As discussed above, the measurements of the yields and spectra of Σ^- and Σ^+ hyperons in heavy ion collisions at different beam energies are expected to provide information on the symmetry energy at high densities. The identification of these hyperons represents an experimental challenge, as their decay lengths are only a few cm, and one of their two decay daughters is a neutral particle. Based on the configuration of the CBM tracking detectors in the magnetic field, the MVD, and the STS, simulations using microscopic transport codes have been performed in order to reconstruct the hyperons by measuring only the hyperon track and the track of the charged decay daughter. The tracks are illustrated in the upper picture of Figure 11 for the case of a Σ^- hyperon decaying into a π^- and a neutron. Based on the missing mass hypothesis, the invariant masses of the Σ^+ and the Σ^- hyperons could be reconstructed, as shown in the lower pictures of Figure 11.

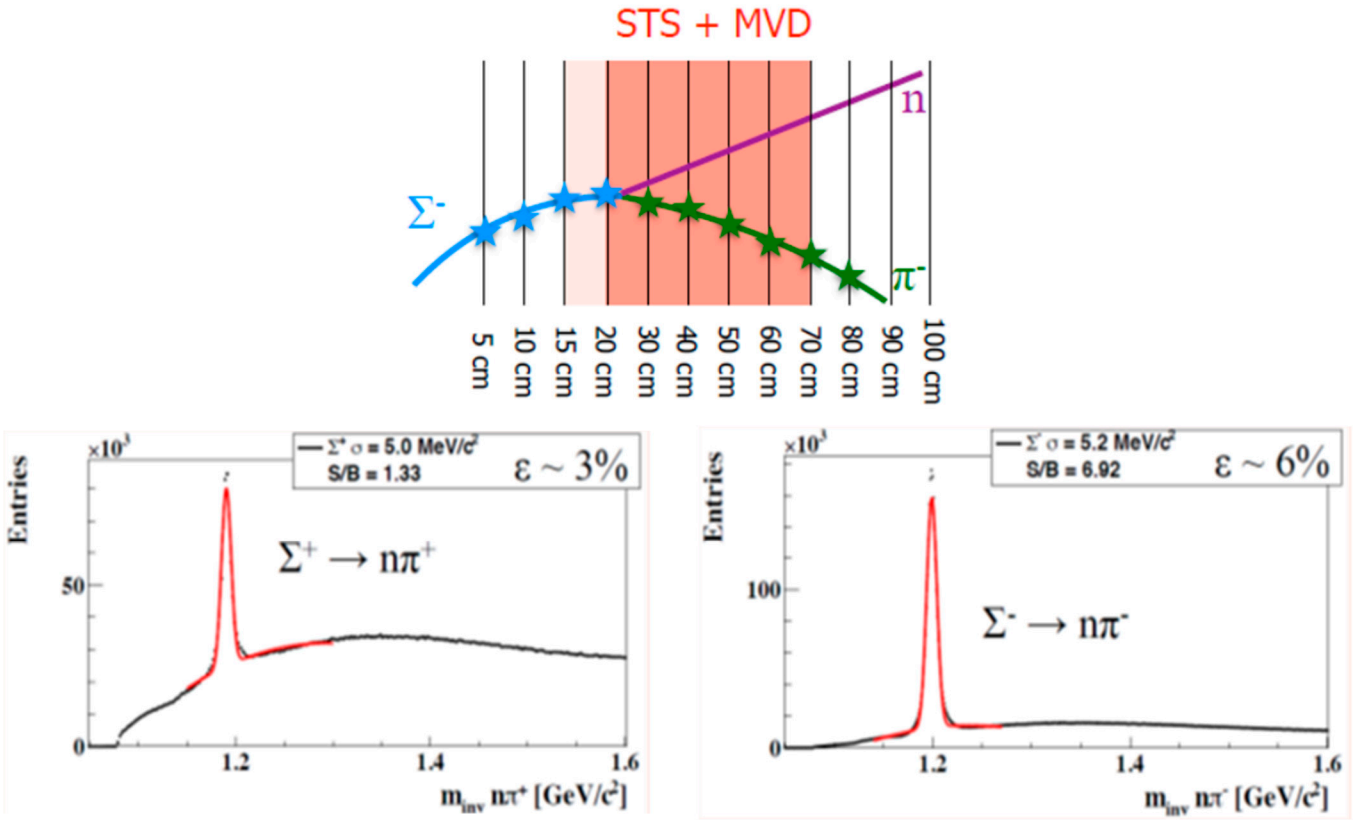

Figure 11. Upper picture: Decay topology of $\Sigma^- \rightarrow n + \pi^-$ together with the hits in the MVD and STS. Left and right lower pictures: Invariant masses of the reconstructed Σ^+ and Σ^- hyperons, respectively.

7. Summary

Laboratory experiments performed in the last decades with heavy ion beams have provided information on the nuclear matter EOS at supranuclear densities, which are relevant for our understanding of the structure of neutron stars and the dynamics of neutron star mergers. A sensitive experimental probe of the EOS is the collective flow of protons and light fragments, which is driven by the pressure gradient in the collision volume. The results of flow measurements at GSI have been analyzed using microscopic transport calculations, indicating a soft EOS for symmetric nuclear matter up to densities of 2 ρ_0. This result was confirmed by the measurement and interpretation of the yields of kaons, which have been studied at several subthreshold energies. From the comparison of the proton and the neutron elliptic flows, constraints for the symmetry energy up to densities of 2 ρ_0 have been extracted. From the proton flow measured up to beam kinetic energies of 10 A GeV, where densities up to about 5 ρ_0 have been reached, only very hard and very soft EOS could be excluded. The interpretation of astronomical observations of the masses and radii of neutron stars, and of gravitational waves from neutron star mergers, results in further constraints on the EOS up to about 4 ρ_0. In this density range, the upcoming CBM experiment at FAIR is designed to measure high-precision data on the collective flow of protons and fragments and on the yields and spectra of multi-strange (anti-) hyperons and hypernuclei and will further restrict the parameter range for the high-density EOS for symmetric nuclear matter and for symmetry energy. Another important field of research will be the exploration of the phase diagram of strongly interacting matter, including the search for the predicted first-order chiral phase transition.

Funding: This research received funding from the Europeans Union's Horizon 2020 research and innovation programme under grant agreement No. 871072.

Data Availability Statement: No new data were created or analyzed in this study.

Conflicts of Interest: The author declares no conflicts of interest.

References

1. Doss, K.G.R.; Gustafsson, H.Å.; Gutbrod, H.H.; Kampert, K.H.; Kolb, B.; Löhner, H.; Ludewigt, B.; Poskanzer, A.M.; Ritter, H.G.; Schmidt, H.R.; et al. Nuclear Collective Flow as a Function of Projectile Energy and Mass. *Phys. Rev. Lett.* **1986**, *57*, 302. [CrossRef]
2. Harris, J.W.; Odyniec, G.; Pugh, H.G.; Schroeder, L.S.; Tincknell, M.L.; Rauch, W.; Stock, R.; Bock, R.; Brockmann, R.; Sandoval, A.; et al. Pion Production in High-Energy Nucleus-Nucleus Collisions. *Phys. Rev. Lett.* **1987**, *58*, 463. [CrossRef]
3. Cubero, M.; Schönhofen, M.; Feldmeier, H.; Nörenberg, W. Delta and pion abundances in hot dense nuclear matter and the nuclear equation of state. *Phys. Lett. B* **1988**, *201*, 11. [CrossRef]
4. Leifels, Y.; Blaich, T.; Elze, T.W.; Emling, H.; Freiesleben, H.; Grimm, K.; Henning, W.; Holzmann, R.; Keller, J.G.; Klingler, H. Exclusive studies of neutron and charged particle emission in collisions of 197Au+ 197Au at 400 MeV/nucleon. *Phys. Rev. Lett.* **1993**, *71*, 963–966. [CrossRef]
5. Ahner, W.; Baltes, P.; Bormann, C.; Brill, D.; Brockmann, R.; Cieślak, M.; Grosse, E.; Henning, W.; Koczoń, P.; Kohlmeyer, B.; et al. KaoS collaboration, Subthreshold kaon production in Au on Au collisions at 1 GeV/u. *Z. Für Phys. A Hadron. Nucl.* **1991**, *341*, 123. [CrossRef]
6. Miśkowiec, D.; Ahner, W.; Barth, R.; Cieślak, M.; Dębowski, M.; Grosse, E.; Henning, W.; Koczoń, P.; Schicker, R.; Schwab, E.; et al. Observation of Enhanced Subthreshold K+ Production in Central Collisions between Heavy Nuclei. *Phys. Rev. Lett.* **1994**, *72*, 3650. [CrossRef]
7. Fuchs, C. Kaon production in heavy ion reactions at intermediate energies. *Prog. Part. Nucl. Phys.* **2006**, *56*, 1–103. [CrossRef]
8. Pinkenburg, C.; Ajitan, N.N.; Alexander, J.M.; Anderson, M.; Best, D.; Brady, F.P.; Case, T.; Caskey, W.; Cebra, D.; Chance, J.L. Elliptic Flow: Transition from Out-of-Plane to In-Plane Emission in Au + Au Collisions. *Phys. Rev. Lett.* **1999**, *83*, 1295. [CrossRef]
9. Danielewicz, P.; Lacey, R.; Lynch, W.G. Determination of the Equation of State of Dense Matter. *Science* **2002**, *298*, 1592. [CrossRef]
10. Le Fèvre, A.; Leifels, Y.; Reisdorf, W.; Aichelin, J.; Hartnack, C. Constraining the nuclear matter equation of state around twice saturation density. *Nucl. Phys. A* **2016**, *945*, 112–133. [CrossRef]
11. Russotto, P.; Gannon, S.; Kupny, S.; Lasko, P.; Acosta, L.; Adamczyk, M.; Al-Ajlan, A.; Al-Garawi, M.; Al-Homaidhi, S.; Amorini, F. Results of the ASY-EOS experiment at GSI: The symmetry energy at supra-saturation density. *Phys. Rev. C* **2016**, *94*, 034608. [CrossRef]
12. Cromartie, H.; Fonseca, E.; Ransom, S.; Demorest, P.; Arzoumanian, Z.; Blumer, H.; Brook, P.; DeCesar, M.; Dolch, T.; Ellis, J.; et al. Relativistic Shapiro delay measurements of an extremely massive millisecond pulsar. *Nat. Astron.* **2019**, *4*, 72. [CrossRef]
13. Antoniadis, J.; Freire, P.; Wex, N.; Tauris, T.; Lynch, R.S.; van Kerkwijk, M.; Kramer, M.; Bassa, C.; Dhillon, V.; Driebe, T.; et al. A Massive Pulsar in a Compact Relativistic Binary. *Science* **2013**, *340*, 448. [CrossRef]
14. Miller, M.; Lamb, F.; Dittmann, A.; Bogdanov, S.; Arzoumanian, Z.; Gendreau, K.; Guillot, S.; Harding, A.; Ho, W.; Lattimer, J.; et al. PSR J0030+0451 Mass and Radius from NICER Data and Implications for the Properties of Neutron Star Matter. *Astrophys. J. Lett.* **2019**, *887*, L24. [CrossRef]
15. Abbott, B.P.; Abbott, R.; Abbott, T.D.; Acernese, F.; Ackley, K.; Adams, C.; Adams, T.; Addesso, P.; Adhikari, R.X.; Adya, V.B.; et al. Multi-messenger Observations of a Binary Neutron Star Merger *. *Astrophys. J. Lett.* **2017**, *848*, L12.
16. Fuchs, C. The Nuclear Equation of State at high densities. *arXiv* **2006**, arXiv:nucl-th/0610038.
17. Blaizot, J.P.; Berger, J.E.; Decharge, J.; Girod, M. Microscopic and macroscopic determinations of nuclear compressibility. *Nucl. Phys. A* **1995**, *591*, 435. [CrossRef]
18. Li, B.A.; Han, X. Constraining the neutron-proton effective mass splitting using empirical constraints on the density dependence of nuclear symmetry energy around normal density. *Phys. Lett. B* **2013**, *727*, 276. [CrossRef]
19. Zhang, Z.; Chen, L.W. Bayesian Inference of the Symmetry Energy and the Neutron Skin in ^{48}Ca and ^{208}Pb from CREX and PREX-2. *Phys. Rev.* **2022**, *108*, 024317.
20. Sturm, C.; Böttcher, I.; Dębowski, M.; Förster, A.; Grosse, E.; Koczoń, P.; Kohlmeyer, B.; Laue, F.; Mang, M.; Naumann, L.; et al. Evidence for a soft nuclear equation of state from kaon production in heavy ion collisions. *Phys. Rev. Lett.* **2001**, *86*, 39. [CrossRef]
21. Fuchs, C.; Faessler, A.; Zabrodin, E.; Zheng, Y.-M. Probing the Nuclear Equation of State by K+ Production in Heavy-Ion Collisions. *Phys. Rev. Lett.* **2001**, *86*, 1974. [CrossRef]
22. Hartnack, C.; Aichelin, J. Analysis of kaon production around the threshold. *J. Phys. G* **2002**, *28*, 1649. [CrossRef]
23. Fuchs, C. The High-Density Equation of State: Constraints from Accelerators and Astrophysics. 2007. Available online: https://pos.sissa.it/047/060 (accessed on 15 May 2024).
24. Russotto, P.; Wu, P.; Zoric, M.M.; Chartier, M.; Leifels, Y.; Lemmon, R.; Li, Q.; Lukasik, J.; Pagano, A.; Pawlowski, P.; et al. Symmetry energy from elliptic flow in ^{197}Au + ^{197}Au. *Phys. Lett. B* **2011**, *697*, 471. [CrossRef]
25. Brown, B.A. Neutron Radii in Nuclei and the Neutron Equation of State. *Phys. Rev. Lett.* **2000**, *85*, 5296. [CrossRef] [PubMed]
26. Tsang, M.; Zhang, Y.; Danielewicz, P.; Famiano, M.; Li, Z.; Lynch, W.; Steiner, A. Constraints on the Density Dependence of the Symmetry Energy. *Phys. Rev. Lett.* **2009**, *102*, 122701. [CrossRef] [PubMed]
27. Horowitz, C.; Brown, E.; Kim, Y.; Lynch, W.; Michaels, R.; Ono, A.; Piekarewicz, J.; Tsang, M.; Wolter, H. A way forward in the study of the symmetry energy: Experiment, theory, and observation. *J. Phys. G Nucl. Part. Phys.* **2014**, *41*, 093001. [CrossRef]
28. Estee, J.; Lynch, W.; Tsang, C.; Barney, J.; Jhang, G.; Tsang, M.; Wang, R.; Kaneko, M.; Lee, J.; Isobe, T.; et al. Probing the Symmetry Energy with the Spectral Pion Ratio. *Phys. Rev. Lett.* **2021**, *126*, 162701. [CrossRef]

29. Wolter, H.; Colonna, M.; Cozma, D.; Danielewicz, P.; Ko, C.M.; Kumar, R.; Ono, A.; Yee, M.; Tsang, B.; Xu, J.; et al. Transport Model Comparison Studies of Intermediate-Energy Heavy-Ion Collisions. *Prog. Part. Nucl. Phys.* **2022**, *125*, 103962. [CrossRef]
30. Li, F.; Chen, L.-W.; Ko, C.M.; Lee, S.-H. Contributions of hyperon-hyperon scattering to subthreshold cascade production in heavy ion collisions. *Phys. Rev.* **2012**, *85*, 064902. [CrossRef]
31. Graef, G.; Steinheimer, J.; Li, L.; Bleicher, M. Deep sub-threshold Ξ and Λ production in nuclear collisions with the UrQMD transport model. *Phys. Rev.* **2014**, *90*, 064909.
32. Aichelin, J.; Bratkovskaya, E.; Le Fevre, A.; Kireyeu, V.; Kolesnikov, V.; Leifels, Y.; Voronyuk, V.; Coci, G. Parton-Hadron-Quantum-Molecular Dynamics (PHQMD)—A Novel Microscopic N-Body Transport Approach for Heavy-Ion Collisions, Dynamical Cluster Formation and Hypernuclei Production. *Phys. Rev.* **2020**, *101*, 044905.
33. Li, Q.; Li, Z.; Zhao, E.; Gupta, R. Σ^-/Σ^+ ratio as a candidate for probing the density dependence of the symmetry potential at high nuclear densities. *Phys. Rev.* **2005**, *71*, 054907.
34. Ding, H.-T.; Hegde, P.; Kaczmarek, O.; Karsch, F.; Lahiri, A.; Li, S.-T.; Mukherjee, S.; Ohno, H.; Petreczky, P.; Schmidt, C.; et al. (Hot QCD Collaboration) Chiral Phase Transition Temperature in (2 + 1)-Flavor QCD. *Phys. Rev. Lett.* **2019**, *123*, 062002. [CrossRef] [PubMed]
35. Basar, G. On the QCD critical point, Lee-Yang edge singularities and Pade resummations. *arXiv* **2023**, arXiv:2312.06952.
36. Gao, F.; Pawlowski, J.-M. QCD phase structure from functional methods. *Phys. Rev.* **2020**, *102*, 034027. [CrossRef]
37. Durante, M.; Indelicato, P.; Jonson, B.; Koch, V.; Langanke, K.; Meißner, U.-G.; Nappi, E.; Nilsson, T.; Stöhlker, T.; Widmann, E.; et al. All the Fun of the FAIR: Fundamental physics at the Facility for Antiproton and Ion Research. *Phys. Scr.* **2019**, *94*, 033001. [CrossRef]
38. Available online: https://fair-center.eu (accessed on 1 January 2022).
39. Senger, P.; Friese, V. The CBM Progress Report 2022, 2023. Available online: https://repository.gsi.de/record/336786 (accessed on 1 January 2022).
40. Vassiliev, I.; Kisel, I. *Multi-Strange Hyperon Reconstruction with the CBM Light Setup*; CBM Progress Report 2019; GSI: Darmstadt, Germany, 2020; ISBN 978-3-9815227-8-5.